Electroconvective instabilities in smectic-C^* liquid crystal films

Stefan Ried,[1] Harald Pleiner,[1,2*] Walter Zimmermann,[3] and Helmut R. Brand[4]
[1]*Universität Essen, FB 7, Physik, D 45117 Essen, Germany*
[2]*Max-Planck-Institut für Polymerforschung, Postfgach 3148, D55021 Mainz, Germany*
[3]*Forschungszentrum Jülich, IFF, D 52425 Jülich, Germany*
[4]*Theoretische Physik III, Universität Bayreuth, D 95440 Bayreuth, Germany*
(Received 7 December 1995)

We investigate the onset of electroconvection in freely suspended smectic-C^* (Sm-C^*) liquid crystal films. Compared to nematic liquid crystals the Sm-C^* phase shows in addition a macroscopic electric polarization within the smectic planes. Describing the Sm-C^* film by a two-dimensional theory we find for low and high frequencies of the applied electric ac field, respectively, a conductive and a dielectric instability regime, similar to the case of electroconvection in nematic liquid crystals. Because of the polarization in the Sm-C^* phase an additional, ''subharmonic regime'' appears at intermediate frequencies, where all the hydrodynamic and electric variables are moving with half the frequency of the applied ac voltage at the onset of convection. For some special but experimentally accessible values of material parameters, geometric dimensions, and ac voltage frequency also a codimension-three point is found, where the threshold voltages of all three possible regimes coincide. For dc voltages the generalized Frederiks transition is presented and discussed as far as it restricts the observation of pattern forming convective instabilities. Both types of instabilities are investigated for dc voltages to get a fundamental insight into the mechanisms involved as well as for ac voltages to stimulate experiments. [S1063-651X(96)00706-4]

PACS number(s): 61.30.−v, 47.20.−k

I. INTRODUCTION

Over the last 20 years of enormous progress in pattern formation, fluid systems have been used as variable model systems, which allow for quantitative investigations far from equilibrium (see, e.g., [1–3]). In the last decade liquid crystals became a paradigm of anisotropic fluids showing pattern forming instabilities (see, e.g., [4–6]). Electroconvection (EC) in planarly aligned nematic liquid crystals is one of these intensively investigated anisotropic systems [5–8].

In chiral smectic liquid crystals (Sm-C^*) a macroscopic polarization exists and Sm-C^* can also be prepared as a quasi two-dimensional (2D) free-standing film [9], similar to free-standing smectic A films [10]. Sm-C^* is an example of a complex fluid with additional macroscopic degrees of freedom, which give rise to different aspects in pattern formation. Here we describe a different convective instability and a generalized Frederiks transition, which both are only possible due to the macroscopic polarization in Sm-C^*. The film geometry chosen will allow in future experimental investigations a detailed observation of the flow field, which is not always possible for the EC in three-dimensional (3D) nematic systems.

Most of the electroconvection experiments in liquid crystals are performed on thin layers of nematics placed between two transparent glass plates at a distance of about 2–200 μm. The orientational order in nematics, described by the director [11], can be fixed in those thin layers along specific directions by preparing the surface of the glass plates in an appropriate manner. Most often the director is aligned parallel to the glass plates (planar geometry). Applying a voltage across the layer the convection sets in above a critical threshold voltage and as a consequence of the optical anisotropy of nematics the patterns can be visualized by using polarized light.

Depending on the frequency of the applied voltage there are two regimes, one at low frequencies (conductive regime) and one at high frequencies (dielectric regime), with different thresholds and critical wavelengths for the cellular convection pattern [8,11,12]. The former is explained by the Carr-Helfrich mechanism [13]: Starting from a uniform alignment of the director a small orientational fluctuation parallel to the glass plates will induce for applied voltages fluctuations of the charge density, since the electric conductivity is anisotropic as well. In the presence of an applied electric field an inhomogeneous charge distribution leads to mass flow, which is coupled to director rotations (flow alignment effect) amplifying the fluctuations under certain conditions for the material parameters. This induced amplification is hindered by the fluid viscosity (and the damping of director rotations) as well as by the orientational elasticity of the director and its fixed orientation at the glass plates. This leads usually to a stationary bifurcation to convective rolls with a wave number q_c at a certain threshold voltage V_c.

At least for some standard substances like MBBA, which shows a nematic phase at room temperature, all important material parameters are known and the influence of the external electric and magnetic fields has been studied extensively in theoretical and experimental work showing qualitative agreement in many cases [5–8]. In contrast to Rayleigh-Bénard convection (driven by a temperature gradient) in isotropic simple or binary fluids, EC (driven by an electric field) of the type discussed here needs an anisotropic fluid with a rotational degree of freedom coupling the preferred direction to the external field. In addition more control parameters are available, since not only the amplitude but also

the frequency of the applied voltage can be varied and because material parameters can easily be tailored within a wide range by mixing different liquid crystal compounds.

In addition to the standard 3D setup for electroconvection in nematics a free-standing film is a promising candidate to gain further insight into the mechanisms of electroconvection. Since free-standing films of nematics are not stable, smectic liquid crystals films have to be used. In the *C* phase the director **n** is tilted with respect to the layer normal (**k**) and its projection onto the layer plane is called the **c**-director. It can be treated as a vector, if all equations are made invariant under the combined replacements $\mathbf{c}\rightarrow-\mathbf{c}$ and $\mathbf{k}\rightarrow-\mathbf{k}$. For the 2D linearized hydrodynamic equations given below this implies that the **c** director behaves like the director of two-dimensional nematic liquid crystal. In the chiral *C** phase (Sm-*C**) a spontaneous polarization exists in each layer (changing its direction helically going from one layer to the next). Such a system has several advantages for EC:

(i) One can choose the geometry of a free-standing film in a way that allows viewing along the direction, which cannot be visualized in the standard 3D nematic setup (i.e., parallel to the glass plates). In freely suspended films the director alignment and the convective flow can be monitored directly using a polarizing microscope. (Sec. II).

(ii) The well defined onset of an instability can serve as an additional means to measure some elastic and viscous material parameters in smectic phases [14], which cannot be obtained directly.

(iii) The macroscopic polarization in Sm-*C** can be used to modify the system by adding different amounts of chiralizing agents. It also provides an additional direct coupling to the external field leading to different physical phenomena (Secs. V and VI).

(iv) Fluctuations of the tilt angle ψ of the director **n** and undulations of the film surface can give rise to different interesting effects in pattern forming instabilities. In this communication, however, such effects will not be considered.

Apart from the Carr-Helfrich mechanism (and its refinements) for EC in anisotropic fluids, there is another mechanism in fluids, based on surface charge layers (''diffusion layers''), that leads to electrohydrodynamic instabilities even in isotropic fluids or isotropic films (i.e., thin smectic-A liquid crystal films [10,15]) and to the ''vortex mode'' pattern above threshold [10]. The influence of this mechanism on EC at very low frequencies of the applied field will be discussed elsewhere. To distinguish the mode explained by Carr-Helfrich from the ''vortex mode'' the former is sometimes called the ''domain mode.''

Since we are mainly interested in the effects of the film geometry and of the macroscopic polarization on EC, we are using here a simplified description assuming fixed smectic layers (i.e., rigid film geometry). As discussed in Sec. III the Sm-*C** phase, which is biaxial for film thicknesses small compared to the pitch, has a larger number of coefficients contained in the material tensors such as the tensors for electric conductivity σ_{ij}^{E}, for the dielectric tensor ϵ_{ij}, for diffusion, for the Soret effect, and for elasticity. However, we neglect this in the following and describe a freely suspended Sm-*C** film as being isomorphic to a two-dimensional nematic with an additional spontaneous electric polarization **P**, which is coupled rigidly to the in-plane director **c**. Thus our description is essentially a 2D nematic one with additional terms in the macroscopic equations due to the polarization. Basic equations are derived in Sec. III.

In Sec. IV a linear stability analysis of the convection-free state is formulated. For applied ac voltages, mainly used in experiments, numerical results are discussed in Sec. VI, while for applied dc voltages a more analytic approach is possible and discussed in Sec. V. The observation of pattern forming instabilities is restricted in some cases by a homogeneous reorientation instability known as the Frederiks transition. We present a generalized ''polarization Frederiks effect'' including torques due to the spontaneous polarization as well as to the dielectric anisotropy ϵ_a. Such a reorientation instability from the planar ground state is now possible for both signs of ϵ_a (and even for $\epsilon_a=0$). A detailed nonlinear analysis of the generalized Frederiks transition is given in Ref. [16].

The known results for nematics [11] are qualitatively unaffected by the presence of the macroscopic polarization for low and high frequencies of the applied electric ac field. At intermediate frequencies, however, a different ''subharmonic regime'' appears as the first unstable mode in Sm-*C**. Its threshold voltage increases with decreasing polarization. For vanishing polarization this regime does not exist and is therefore not accessible in other liquid crystal phases such as nematics or smectic *C*. Under certain conditions a codimension-three point is found, where the three different instabilities (conductive, dielectric, and subharmonic, all with different wavelengths and different temporal behavior) compete at onset.

II. GEOMETRIES

The geometry of the physical situation of interest here is sketched in Fig. 1. In contrast to the nematic phase the smectic phases are organized in layers. In the smectic-*C* phase the director **n** is tilted by a fixed angle ψ relative to the layer normal **k**. So the only hydrodynamic degree of freedom of the director alignment is a rotation θ around **k**. The projection of **n** onto the plane of the smectic layers is the **c** director, which can be observed by polarized light normal to the layer. Due to the existence of **k** and **c** this phase is biaxial.

In contrast to the Sm-*C* phase the Sm-*C** phase shows an intrinsic twist of the director from layer to layer. This additional symmetry breaking ($C_{2h}\rightsquigarrow C_2$ locally) allows microscopic electric dipoles to form a spontaneous electric polarization **P**, which lies in the planes (perpendicular to both **k** and **c**) and is twisted, too. We will neglect this twist in the following thus assuming that the thickness of the freely suspended film is small compared to the pitch of the helielectric *C** phase [9], which is typically $\sim 1-10\ \mu$m.

Thus we consider as the ground state (without applied voltage) a homogeneous structure, where each **P** and **c** have on average one specific preferred direction, perpendicular to each other. Since we assume the layers to be rigid, we can use a 2D model to describe the system. The first and last few layers (at the free surface) might be deformed and might form higher ordered smectic phases. We neglect those effects here and consider their influence elsewhere.

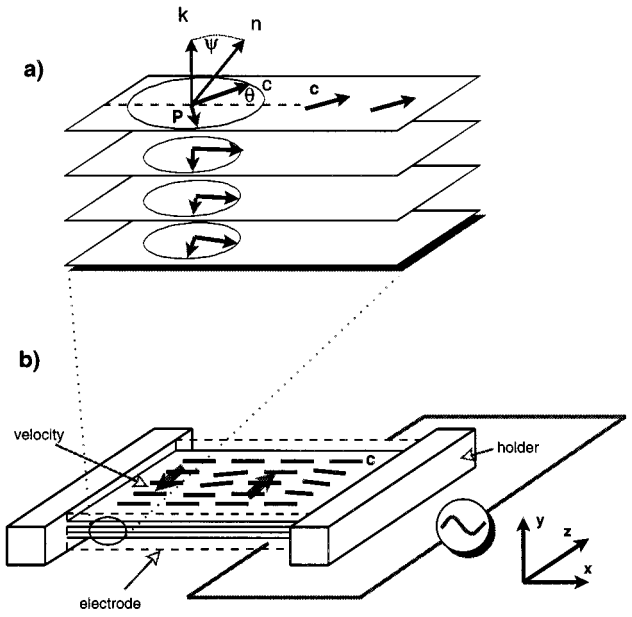

FIG. 1. (a) A stack of Sm-C^* layers is shown, for which the orientation of the director **n** changes from layer to layer gradually. (b) Similarly to experiments with Sm-A films [17] we suggest the sketched experimental setup for the study of electroconvection in Sm-C^*-films. A rectangular freely suspended Sm-C^* film is plotted with the electrodes parallel to the x direction. The length of the film is assumed to be much longer ($\|x$) than wide ($\|z$).

III. BASIC EQUATIONS

A systematic approach to electrohydrodynamics in liquid crystals is presented in Ref. [18]. The origin of hydrodynamic variables are either conservation laws or spontaneously broken symmetries. In the smectic-C phase translational symmetry along the layer normal and rotational symmetry about the layer normal are broken and, thus, layer displacement (along its normal) and in-plane rotations of the **c** vector are the hydrodynamic variables in addition to those (mass density ρ, momentum density **g**, and energy density ϵ) already present in isotropic liquids. Since the Carr-Helfrich mechanism requires the presence of free charges, electric charge (ρ_e) conservation has to be considered.

Since the film geometry we have in mind is approximately a 2D situation, we already reduce the full three-dimensional formulation of the equations to a two-dimensional one. We follow the notation of Refs. [19–22] to write down the conservation of charge and momentum as well as the director balance equation (incompressibility assumed). In the following we assume isothermal conditions and a single component liquid crystal.

The in-plane spontaneous polarization **P**

$$\mathbf{P}=p_0(\sin\theta,0,-\cos\theta) \tag{3.1}$$

is always perpendicular to the **c** director

$$\mathbf{c}=(\cos\theta,0,\sin\theta), \tag{3.2}$$

where the angle θ describes the orientation within the film plane. The **c** director is the projection of the **n** director

$$\mathbf{n}=(\sin\psi\,\cos\theta,\cos\psi,\sin\psi\,\sin\theta), \tag{3.3}$$

where the angle ψ describes the tilt of **n** with respect to **k**.

The charge conservation is described by

$$\partial_t\rho_e+\mathrm{div}\mathbf{j}=0, \tag{3.4}$$

where ∂_t is the partial time derivative. The electric current density results from the convective charge transport (due to the velocity field v_i), from conduction (due to the electric field **E**), and from (dissipative) dynamic flexoelectricity [due to the molecular field, cf. Eq. (3.13) below]

$$j_i=\rho_e v_i+\sigma^E_{ij}E_j+\nabla_j(\zeta^E_{kji}h_k). \tag{3.5}$$

The electric conductivity is one of the symmetric second rank material tensors, which in Sm-C (and Sm-C^* locally) have four different components

$$\sigma^E_{ij}=\sigma_1k_ik_j+\sigma_2(\delta_{ij}-k_ik_j)+\sigma_3n_in_j+\tfrac{1}{2}\sigma_4(n_ik_j+n_jk_i). \tag{3.6}$$

In our 2D description only two coefficients are relevant and all the second rank material tensors are of the form

$$\sigma^E_{ij}=\sigma_\perp\delta_{ij}+\sigma_ac_ic_j=\sigma_\perp\delta^{tr}_{ij}+\sigma_\parallel c_ic_j, \tag{3.7}$$

where $\delta^{tr}_{ij}\equiv\delta_{ij}-c_ic_j$ and $\sigma_a\equiv\sigma_\parallel-\sigma_\perp$, with $\sigma_\perp=\sigma_2$ and $\sigma_a=\sigma_3\sin^2\psi$. For the structure of the dynamic flexoelectric tensor ζ^E_{ijk} see Ref. [18].

The (Legendre transformed) electric energy density is given by

$$f_e=-\tfrac{1}{2}\epsilon_{ij}E_iE_j-P_iE_i+\tilde{e}_{kji}E_i\nabla_kc_j, \tag{3.8}$$

from which the dielectric displacement is obtained as a sum of the field contribution E_i, the spontaneous polarization P_i, and the static flexoelectric part (the latter will be neglected below)

$$D_i=-\frac{\delta f_e}{\delta E_i}=\epsilon_{ij}E_j+P_i-\tilde{e}_{kji}\nabla_kc_j. \tag{3.9}$$

The electric field itself $\mathbf{E}=\mathbf{E}_0-\boldsymbol{\nabla}\phi$ can be decomposed into the external field $\mathbf{E}_0$ (along the z direction in the following) due to the applied voltage V

$$E_0(t)=\frac{V(t)}{d}\quad\text{with}\quad V(t)=V_0a(t) \tag{3.10}$$

and the gradient of the induced electric potential ϕ. This fulfills the first quasistatic Maxwell equation curl$\mathbf{E}=0$, while the second one, div$\mathbf{D}=\rho_e$ can be used to eliminate ρ_e from Eq. (3.5).

The balance equation of the director [19,20,22] is written here in the 2D form

$$\dot{c}_i+Y_i=0. \tag{3.11}$$

The quasicurrent Y_i contains a reactive part due to flow and a dissipative part due to gradients of **c** and **E** and Eq. (3.11) reads

$$\partial_t c_i + (\mathbf{v}\cdot\nabla)c_i = \zeta^E_{ijk}\nabla_j E_k + \delta^{tr}_{ik}\left[\frac{1}{2}(1+\lambda)c_j\nabla_j v_k + \frac{1}{2}(\lambda-1)c_j\nabla_k v_j + \frac{1}{\gamma_1}h_k\right], \quad (3.12)$$

showing a coupling of director rotations to rotational flow, to elongational flow (via the dimensionless flow alignment parameter λ) and to the molecular field h_i (via the the rotational viscosity γ_1). The dynamic flexoelectric effect ($\sim\zeta^E_{ijk}$) will be neglected below. The molecular field h_i is the variational derivative of the free energy density f,

$$h_i = -\frac{\delta f}{\delta c_i} = -\frac{\partial f}{\partial c_i} + \nabla_j \frac{\partial f}{\partial \nabla_j c_i}, \quad (3.13)$$

with $f = f_F + f_e$ the sum of rotational elasticity f_F, [11]

$$f_F = \tfrac{1}{2}K_1(\mathrm{div}\mathbf{c})^2 + \tfrac{1}{2}K_2(\mathbf{c}\cdot\mathrm{curl}\mathbf{c})^2 + \tfrac{1}{2}K_3(\mathbf{c}\times\mathrm{curl}\mathbf{c})^2, \quad (3.14)$$

and the electric energy density f_e from Eq. (3.8). The momentum conservation,

$$\rho_m(\partial_t + (\mathbf{v}\cdot\boldsymbol{\nabla}))v_i = \nabla_l(\sigma^R_{il} + \sigma^D_{il}) + (\boldsymbol{\nabla}\cdot\mathbf{D})E_i, \quad (3.15)$$

includes the electric volume force on induced and spontaneous polarizations in the media due to the definition of the dielectric displacement in Eq. (3.9). The reversible part of the stress tensor is

$$\sigma^R_{ij} = -p\,\delta_{ij} - \tfrac{1}{2}([\lambda+1]\delta^{tr}_{ik}c_j + [\lambda-1]\delta^{tr}_{jk}c_i)h_k, \quad (3.16)$$

where p is the hydrostatic pressure. The irreversible part of the stress tensor is [20]

$$\sigma^D_{ij} = 2\nu_2 A_{ij} + 2(\nu_1+\nu_2-2\nu_3)c_ic_jc_kc_lA_{kl} + 2(\nu_3-\nu_2) \times(A_{ik}c_kc_j + A_{jk}c_ic_k) + (\nu_5-\nu_4+\nu_2)\delta_{ij}c_kc_lA_{kl}, \quad (3.17)$$

where $2A_{ij} = \nabla_i v_j + \nabla_j v_i$ has been used and incompressibility,

$$\mathrm{div}\mathbf{v} = 0, \quad (3.18)$$

has been assumed. The thermal degree of freedom will be neglected, since generally it does not play a role in EC.

IV. LINEAR ANALYSIS

A. Linearized equations

In the following we will investigate the linear stability of the homogeneous and convection-free planar basic state $\theta=0$, $\mathbf{v}=0$ and $\phi=0$ (i.e., $\mathbf{c}$ is in x and $\mathbf{E}_0$ in z direction), which is stable at voltages V below a certain threshold value. Therefore we linearize our system of equations around the basic state and consider the dynamics of the small deviations θ, $\mathbf{v}$, and ϕ. Due to the 2D description there are no gradients in the y direction and all vector fields have vanishing y components (i.e., $v_y=0$). The component v_x is expressed by v_z via the incompressibility condition (3.18). The pressure is obtained by taking the divergence of Eq. (3.15), but it will not be needed.

We consider a film that is infinitely extended in the x direction (or periodic boundary conditions) and we can therefore treat the x dependence of the linearized equations of motion by a Fourier ansatz

$$\phi(x,z,t) = \sin(qx)\,\tilde{\phi}(z,t),$$
$$v_z(x,z,t) = \sin(qx)\,\tilde{v}_z(z,t), \quad (4.1)$$
$$\theta(x,z,t) = \cos(qx)\,\tilde{\theta}(z,t).$$

After some straightforward algebra we obtain three linear equations of motion for the fields $\tilde{\phi}(z,t)$, $\tilde{v}_z(z,t)$ and $\tilde{v}_z(z,t)$. Dropping the ''tilde'' for simplicity the equation corresponding to the charge conservation for example is:

$$(\epsilon_\parallel q^2 - \epsilon_\perp\nabla_z^2)\partial_t\phi - [\epsilon_a E_0(t) - p_0]q\,\partial_t\theta + (\sigma_\parallel q^2 - \sigma_\perp\nabla_z^2)\phi - \{\epsilon_a[\partial_t E_0(t)] + \sigma_a E_0(t)\}q\,\theta = 0. \quad (4.2)$$

In order to rewrite the equations in a dimensionless form we rescale all lengths by the film width d, i.e.,

$$x = x'\frac{d}{\pi}. \quad (4.3)$$

While frequently time is scaled by the charge relaxation time $\epsilon_\perp/\sigma_\perp$, we choose instead the following rescaling for time, voltage, and mass density, respectively,

$$t = t'\tau_0 = t'\frac{\gamma_1 d^2}{K_1\pi^2}, \quad (4.4)$$

$$V = V'\pi\left(\frac{K_1}{\epsilon_\perp}\right)^{1/2}, \quad (4.5)$$

$$\rho_m = \rho'_m\frac{\gamma_1^2}{K_1} \quad (4.6)$$

so, if the film width d is varied, only rescaled conductivities $\sigma'_\perp, \sigma'_\parallel$, and p'_0 must be changed (cf. Sec. VI D).

For the variables this implies the dimensionless (primed) forms

$$\phi' = \phi\left(\frac{\epsilon_\perp}{K_1}\right)^{1/2}, \quad (4.7)$$

$$v'_z = v_z\frac{\gamma_1 d}{K_1\pi}, \quad (4.8)$$

$$\theta' = \theta, \quad (4.9)$$

while q, ∇_z, and ∂_t scale inversely to Eqs. (4.3) and (4.4), respectively. In order to simplify the resulting equations we introduce the dimensionless abbreviations

$$\sigma'_{\parallel,\perp} = \sigma_{\parallel,\perp}\frac{d^2}{\pi^2}\frac{\gamma_1}{\epsilon_\perp K_1}, \quad (4.10)$$

$$p_0' = p_0 \frac{d}{\pi} (\epsilon_\perp K_1)^{-(1/2)}. \tag{4.11}$$

Dropping the primes *everywhere* for notational simplicity, the linearized dimensionless equations then read

$$0 = \left(\frac{\epsilon_\parallel}{\epsilon_\perp} q^2 - \nabla_z^2 \right) \partial_t \phi + \left(- \frac{\epsilon_a}{\epsilon_\perp} V(t) + p_0 \right) q \partial_t \theta + (\sigma_\parallel q^2 - \sigma_\perp \nabla_z^2) \phi + \left(- \frac{\epsilon_a}{\epsilon_\perp} [\partial_t V(t)] - \sigma_a V(t) \right) q \theta, \tag{4.12}$$

$$0 = - \partial_t \theta + \left(p_0 - \frac{\epsilon_a}{\epsilon_\perp} V(t) \right) q \phi - \frac{1}{q} (\alpha_2 q^2 + \alpha_3 \nabla_z^2) v_z + \left(\frac{\epsilon_a}{\epsilon_\perp} V^2(t) - p_0 V(t) - \frac{K_3}{K_1} q^2 + \nabla_z^2 \right) \theta, \tag{4.13}$$

$$0 = \rho_m (q^2 - \nabla_z^2) \partial_t v_z + q (\alpha_2 q^2 + \alpha_3 \nabla_z^2) \partial_t \theta + \left(\nabla_z^2 - \frac{\epsilon_\parallel}{\epsilon_\perp} q^2 \right) q^2 V(t) \phi + \left(\frac{\epsilon_a}{\epsilon_\perp} V^2(t) - p_0 V(t) \right) q^3 \theta + (\eta_c q^4 - 2 \hat{\eta} q^2 \nabla_z^2 + \eta_b \nabla_z^4) v_z. \tag{4.14}$$

In Eq. (4.14) the molecular field h_i has been eliminated via Eq. (4.13). The external field E_0 has been replaced by the external applied voltage V, with $V = E_0$ for dimensionless quantities. In addition we have used the abbreviations (in order to make contact with the notation in nematic EC) in the dimensionless rescaling:

$$2\alpha_2 = -1 - \lambda,$$

$$2\alpha_3 = 1 - \lambda,$$

$$\eta_b = \frac{\nu_3}{\gamma_1} + \frac{1}{4}(1-\lambda)^2, \tag{4.15}$$

$$\eta_c = \frac{\nu_3}{\gamma_1} + \frac{1}{4}(1+\lambda)^2,$$

$$\hat{\eta} = \frac{1}{\gamma_1}(\nu_1 + \nu_2 - \nu_3) + \frac{1}{4}(1-\lambda^2).$$

We are left with three homogeneous linear partial differential equations for θ, v_z and ϕ. They are similar to the linear equations for planarly aligned nematic liquid crystals [12,23], but contain, in addition, the effects of the polarization p_0. Equations (4.12-4.14) can be written in matrix form,

$$\mathsf{B}(t, \nabla_z) \cdot \partial_t \mathbf{u}(z,t) = \mathsf{L}(t, \nabla_z) \cdot \mathbf{u}(z,t), \tag{4.16}$$

with the (formal) vector field:

$$\mathbf{u} = (\phi, \theta, v_z). \tag{4.17}$$

We always assume dc or periodic ac driving voltages. For periodic voltages $V(t) = V(t+T)$, with $T = 2\pi/\omega$, the matrices B and L are periodic in time and Eq. (4.16) shares some similarities with the well known Matthieu equations. In the following we assume additionally

$$V(t + T/2) = -V(t). \tag{4.18}$$

B. Boundary conditions

We consider films infinitely extended in x direction (or take periodic boundary conditions). In z direction the film is confined between electrodes located at $z = \pm(\pi/2)$, with the following consequences. The velocity v_z perpendicular to the electrodes has to vanish at this surface:

$$v_z \left(\pm \frac{\pi}{2} \right) = 0 . \tag{4.19}$$

In addition stress-free boundary conditions,

$$\partial_z^2 v_z \left(\pm \frac{\pi}{2} \right) = 0 , \tag{4.20}$$

or rigid boundary conditions

$$\partial_z v_z \left(\pm \frac{\pi}{2} \right) = 0, \tag{4.21}$$

are assumed, where the latter case is closer to the real experimental conditions.

At the surface we assume the director $\mathbf{c}$ to lie, on average, in one direction [$\mathbf{c} = (1,0,0)$] and the induced potential to be zero:

$$\theta \left(\pm \frac{\pi}{2} \right) = 0, \quad \phi \left(\pm \frac{\pi}{2} \right) = 0 . \tag{4.22}$$

C. Symmetries and Floquet analysis

The solutions of the linearized Eqs. (4.12–4.14) can be classified with respect to their symmetry properties under spatial reflections and translations in time. Choosing the line $z = 0$ to be the middle of the film, i.e., $-\pi/2 < z < \pi/2$, where π is the rescaled film width in Fig. 1, Eq. (4.16) is invariant under a reflection with respect to the z direction.

$$z \rightarrow -z. \tag{4.23}$$

This symmetry of the equations together with the boundary conditions chosen allows us to characterize all solutions to be either symmetric $\mathbf{u}(z) = \mathbf{u}(-z)$, or antisymmetric, $\mathbf{u}(z) = -\mathbf{u}(-z)$, with respect to z. This would not be possible, if we had kept the flexoelectric effect related to $\tilde{e}_{ijk}$ in Eqs. (3.8) and (3.9) [12] and its dynamic analog $\sim \zeta^E_{ijk}$ in Eqs. (3.5) and (3.12).

For periodic voltages as given in Eq. (4.18), the linear homogeneous Eq. (4.16) is invariant under the time translations:

$$t \rightarrow t + nT \quad (n \text{ integer, positive}). \tag{4.24}$$

According to the spectral method of Floquet [24] this leads to a general solution of the form

$$\mathbf{u}(z,t) = \hat{\mathbf{u}}(z,t) e^{\sigma t}, \tag{4.25}$$

with the Floquet exponent σ and the periodic function $\hat{\mathbf{u}}$. Due to the symmetry (4.24) the solutions $\hat{\mathbf{u}}$ are grouped according to the integers n into harmonic ones ($n=1$), subharmonic ones ($n=2$), etc. The harmonic ones are invariant under a single T-translation $t\to t+T$, i.e., $\hat{\mathbf{u}}(t)=\hat{\mathbf{u}}(t+T)$, while the subharmonic ones change sign $\hat{\mathbf{u}}(t)=-\hat{\mathbf{u}}(t+T)$ under that translation. The full solutions $\mathbf{u}(t)$ do not have these symmetries because of the Floquet multiplier $\exp(\sigma t)$. However the prefactors produced by a time translation, i.e., $\exp(\sigma T)$ for a T translation, are irrelevant, since the amplitudes of the solutions $\mathbf{u}(t)$ are not determined by the linear, homogeneous equation (4.16).

The Floquet exponent σ is a function of the external (V_0, ω) and internal (material) parameters of the system and depends on the transverse wave vector q. It governs the linear stability of the basic, nonconvective state against inhomogeneous perturbations $\mathbf{u}$, which is stable, if $\mathrm{Re}(\sigma)<0$, and unstable for positive growth rates $\mathrm{Re}(\sigma)>0$. Thus from the condition

$$\mathrm{Re}[\sigma(V_0,q,\ldots)]=0 \tag{4.26}$$

the parameters can be determined which separate the linear stable regime from the unstable one. Equation (4.26) allows for instance the determination of V_0 as a function of q, the so-called neutral curve $V_0(q)$ at which the real part of the Floquet exponent changes its sign. The absolute minimum of $V_0(q)$, $V_c=V_0(q_c)$, gives the threshold for the onset of convection in linearized stability analysis.

For vanishing p_0 (Sm-C phase) as well as for T periodic and antisymmetric ac voltages [cf. (4.18)], e.g., sinusoidal, square, or triangular wave forms, there is an additional symmetry with respect to time translations, since Eq. (4.16) is invariant under the replacement,

$$t\to t+\frac{T}{2},\quad \text{if}\quad \begin{pmatrix}\phi\\ \theta\\ v_z\end{pmatrix}\to\pm\gamma\begin{pmatrix}-\phi\\ \theta\\ v_z\end{pmatrix}, \tag{4.27}$$

where γ is an irrelevant constant. This symmetry requires the solutions $\hat{\mathbf{u}}$ to be harmonic, since by applying (4.27) twice (i.e., after a T translation) $\hat{\mathbf{u}}$ is mapped to itself. Thus, if Eq. (4.27) is valid, subharmonic solutions are ruled out. The upper and lower signs in (4.27) belong to two different solutions, corresponding to the so-called conductive and dielectric regime, respectively, known from EC in nematic liquid crystals [11]. In Sm-C^* however, this symmetry (4.27) is lifted, since $p_0\neq 0$. In that case subharmonic solutions are possible and the two harmonic regimes can still be discriminated, but they are no longer purely ''conductive'' nor purely ''dielectric.''

D. Mode ansatz

For the actual determination of the eigenvalues σ we transform Eq. (4.16) into a system of linear algebraic equations by choosing an appropriate representation of the periodic part of the solution (4.25) function, $\hat{\mathbf{u}}(z,t)$. Most often, $\hat{\mathbf{u}}$ is assumed to have the same period as the driving voltage. However, bifurcation to nT-periodic solutions (n integer, >1) is also possible, where generally only the subharmonic (period doubled) case $n=2$ gives stable solutions [24]. In this state the basic time translational symmetry $t\to t+T$ is broken spontaneously. Therefore, we make the ansatz

$$\hat{\mathbf{u}}=\sum_{l=-N}^{N}\mathbf{u}_l(z)\exp\left(il\frac{\omega}{2}t\right). \tag{4.28}$$

which contains both, the T-periodic, harmonic ($l=\pm 2$), and the $2T$-periodic, subharmonic ($l=\pm 1$) solutions as well as all their higher harmonics (l = even or odd, respectively) and even time independent ones.

The dependence on z is expressed by a complete set of orthogonal functions according to the boundary conditions chosen. The z dependence of $\phi(z)$ as well as $\theta(z)$ can be described appropriately by an expansion with respect to trigonometric functions:

$$f_m(z)=\begin{cases}\cos(mz), & m=1,3,5,\ldots\\ \sin(mz), & m=2,4,6,\ldots\end{cases}. \tag{4.29}$$

Each of it fulfills the boundary conditions in Eq. (4.22). For stress-free boundary conditions (4.20) this expansion is also appropriate for the velocity field $v_z(z)$ and Eq. (4.16) is solved by

$$\hat{\mathbf{u}}=\sum_{l=-N}^{N}\sum_{m=1}^{M}\mathbf{U}_{lm}\exp\left(il\frac{\omega}{2}t\right)f_m(z). \tag{4.30}$$

The (vector) coefficient matrix $\mathbf{U}_{lm}=(P_{lm},T_{lm},G_{lm})$ consists of three components according to the three components of $\hat{\mathbf{u}}=(\phi,\theta,v_z)$.

For rigid boundary conditions the ansatz $\{f_m(z)\}$ for the velocity field does not satisfy Eq. (4.21) and has to be replaced by symmetric and antisymmetric Chandrasekhar functions [10,25],

$$r_m(z)=\begin{cases}\dfrac{\cosh(\lambda_m z/\pi)}{\cosh(\lambda_m/2)}-\dfrac{\cos(\lambda_m z/\pi)}{\cos(\lambda_m/2)}, & m=1,3,\ldots\\ \dfrac{\sinh(\lambda_m z/\pi)}{\sinh(\lambda_m/2)}-\dfrac{\sin(\lambda_m z/\pi)}{\sin(\lambda_m/2)}, & m=2,4,\ldots,\end{cases} \tag{4.31}$$

where in λ_m the roots of the characteristic equations

$$\tanh(\lambda/2)+\tan(\lambda/2)=0\rightsquigarrow\lambda_1,\lambda_3,\ldots, \tag{4.32}$$

$$\coth(\lambda/2)-\cot(\lambda/2)=0\rightsquigarrow\lambda_2,\lambda_4,\ldots, \tag{4.33}$$

are collected in an alternating manner. This leads to rigid boundary conditions instead of (4.30) to the ansatz for v_z:

$$v_z(x,z,t)=e^{\sigma t}\sum_{l=-N}^{N}\sum_{m=1}^{M}G_{lm}\exp\left(il\frac{\omega}{2}t\right)r_m(z). \tag{4.34}$$

Inserting the mode expansions (4.28) and/or (4.34) into the linearized equation (4.16) and projecting onto the respective eigenmodes $\exp(il\omega/2\,t)r_m(z)$ and $\exp(il(\omega/2\,t)f_m(z)$, we obtain algebraic equations linear in the coefficients P_{lm},T_{lm},G_{lm}.

Defining a $3M(2N+1)$-dimensional vector $\mathbf{X}$ containing all components of $\mathbf{U}_{lm}$ in an arbitrary sequential order, e.g.,

$$\mathbf{X}=(P_{-N,1},P_{-N+1,1},\ldots,P_{N,1},P_{-N,2},P_{-N+1,2},\ldots,P_{N,2},\ldots,\ldots,P_{N,M},T_{-N,1},\ldots,\ldots,T_{N,M},G_{-N,1},\ldots,\ldots,G_{N,M}), \tag{4.35}$$

the set of linear algebraic equations is of the following symbolic form:

$$\sigma \mathsf{B}_1\cdot\mathbf{X}+i\omega\mathsf{B}_2\cdot\mathbf{X}=\mathsf{L}_1\cdot\mathbf{X}. \tag{4.36}$$

Here the matrices B_1, B_2 and L_1 are 3×3 block matrices, where each block itself is a $M(2N+1)\times M(2N+1)$ matrix. The matrices B_1 and L_1 result from B and L from Eq. (4.16), respectively, while B_2 contains elements of both, B and L, because of the explicit time derivative of the external voltage contained in Eq. (4.12).

Since mixed projection integrals of even and odd functions in space or in time, respectively, vanish identically, the system (4.36) will only contain equations coupling even components to each other and odd components to each other. In the time expansion even and odd corresponds to harmonic and subharmonic modes while in the expansion in the z direction even components are linked to antisymmetric functions and odd ones to symmetric functions [cf. Eq. (4.29,4.31)]. Thus the eigenvector of a marginally stable mode contains components out of one of the following modes only:

$$\mathbf{X}=\{(\mathbf{U}_{\text{harm,anti}}),(\mathbf{U}_{\text{harm,sym}}),(\mathbf{U}_{\text{subh,anti}}),(\mathbf{U}_{\text{subh,sym}})\}. \tag{4.37}$$

In Eqs. (4.28,4.30,4.34) we have already truncated the infinite sums to finite ones taking into account only $2N+1$ temporal and M spatial modes. This approximation is justified as the amplitude of the corresponding components decreases extremely fast for $N>8$ and $M>6$ (the Galerkin approximation). All matrices depend on the yet undetermined transverse wave vector q and on the amplitude V_0 of the applied voltage, which we will take as sinusoidal, $V(t)=V_0\cos(\omega t)$ or constant, $V(t)=V_0$, in the following.

V. dc INSTABILITIES

Before presenting the results for applied ac voltages in Sec. VI, we will discuss the special case of a time-independent applied voltage $V(t)=V_0$. Although experimentally less important than the ac case, because of charge injection problems, it nevertheless is simple enough to discuss the influence of p_0 on the nature of the instabilities.

A. dc polarization Frederiks effect

In addition to EC instabilities ($q_c\neq0$), nematic liquid crystals can also become unstable against a purely orientational instability, if subject to external electric (or magnetic) fields. This well-known Frederiks transition [11,26] has the minimum of the neutral curve at $q_c=0$, describing a static reorientation of the director (which is homogeneous in the x direction) without any flow. The mechanism is based on the dielectric (or magnetic) susceptibility anisotropy, which favors an alignment of the director field parallel or perpendicular to the applied field depending on the sign of the susceptibility anisotropy ($\epsilon_a>0$ or $\epsilon_a<0$), while orientational elasticity works to preserve the original orientation of the director field.

This type of instability is also present in smectic-C films ($p_0=0$) and the critical voltage for an electrically driven splay Frederiks transition can be obtained from Eq. (4.13) with $q=v_z=\phi=0$ and $\theta=\bar{\theta}\cos(z)$ reading (in our dimensionless units)

$$V_c^2=\epsilon_\perp/\epsilon_a. \tag{5.1}$$

A threshold value and therefore an electrically driven splay Frederiks transition exist only for finite positive values of ϵ_a, since in our basic state $\mathbf{c}\perp\mathbf{E}$.

In this case ($p_0=0$) the sign of the dc voltage is arbitrary, since an applied electric field $\mathbf{E}$ is completely equivalent to $-\mathbf{E}$. Thus the threshold for the splay Frederiks instability depends on V_0^2 only. This behavior is changed qualitatively in smectic-C^* due to the presence of the polarization $\mathbf{P}$. There is an orientational effect of the field on the polarization and $\mathbf{E}$ parallel to $\mathbf{P}$ ($V_0>0$) is energetically preferred to the case $\mathbf{E}$ antiparallel to $\mathbf{P}$ ($V_0<0$) (cf. Fig. 1). Thus, even for vanishing dielectric anisotropy, $\epsilon_a=0$, one finds an orientational transition of the Frederiks type (''polarization Frederiks effect'') at the threshold $V_c=-1/p_0$. This instability only occurs, if the spontaneous polarization and the applied electrical field are antiparallel to each other ($V_0<0$).

In the general case, i.e., for finite values of p_0 and ϵ_a, both orientational torques are present and the threshold formula of the general Frederiks instability ($\phi=v_z=q=0$) due to an applied dc voltage is

$$V=\frac{\epsilon_\perp p_0}{2\epsilon_a}\left[1\pm\left(1+4\frac{\epsilon_a}{p_0^2\epsilon_\perp}\right)^{1/2}\right]. \tag{5.2}$$

This formula contains both, the traditional splay Frederiks effect (due to dielectric torques) and the new ''polarization Frederiks effect'' (due to ferroelectric torques). Since polarization and director are rigidly coupled, both effects can either enhance each other (for $V_0<0$ and $\epsilon_a>0$) and therefore reduce the threshold voltage [cf. the lower dotted line in Fig. 2(b)], or counteract each other (for $V_0>0$ and $\epsilon_a>0$) increasing the threshold voltage [cf. the upper dotted line in Fig. 2(b)].

In contrast to the traditional splay Frederiks transition that does not exist for $\epsilon_a<0$, the general Frederiks transition can exist even for $\epsilon_a<0$, if $V_0<0$ (external field antiparallel to the polarization) and if p_0 exceeds a critical value $p_0>p_c$, where

$$p_c=(-4\epsilon_a/\epsilon_\perp)^{1/2}. \tag{5.3}$$

In that case the destabilizing effect due to the polarization overcomes the stabilizing effects due to the dielectric anisotropy. This range is shown in Fig. 3(b), where below the dotted curve the planar initial configuration is unstable against homogeneous reorientation of the director field.

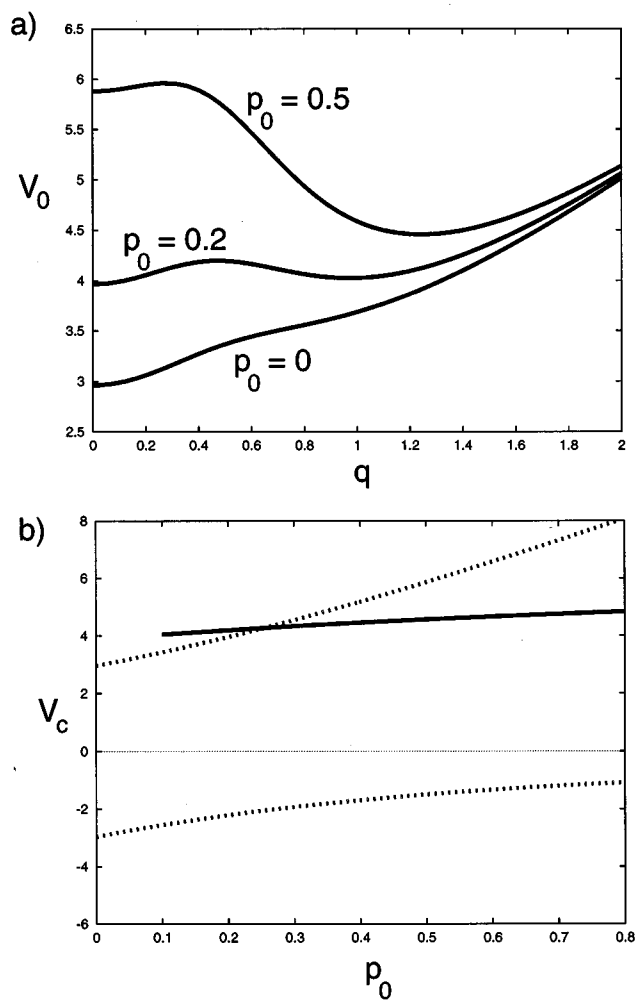

FIG. 2. (a) The neutral curve for $\epsilon_a = +0.6\epsilon_0$ without polarization ($p_0 = 0$) and with a polarization $p_0 = 0.2$ and $p_0 = 0.5$ parallel to the applied field ($V_0 > 0$). In (b) the threshold of electroconvection (solid lines) is compared with the that of the Frederiks transition (dotted lines) as a function of the polarization (for the positive value of $\epsilon_a = 0.6\epsilon_0$).

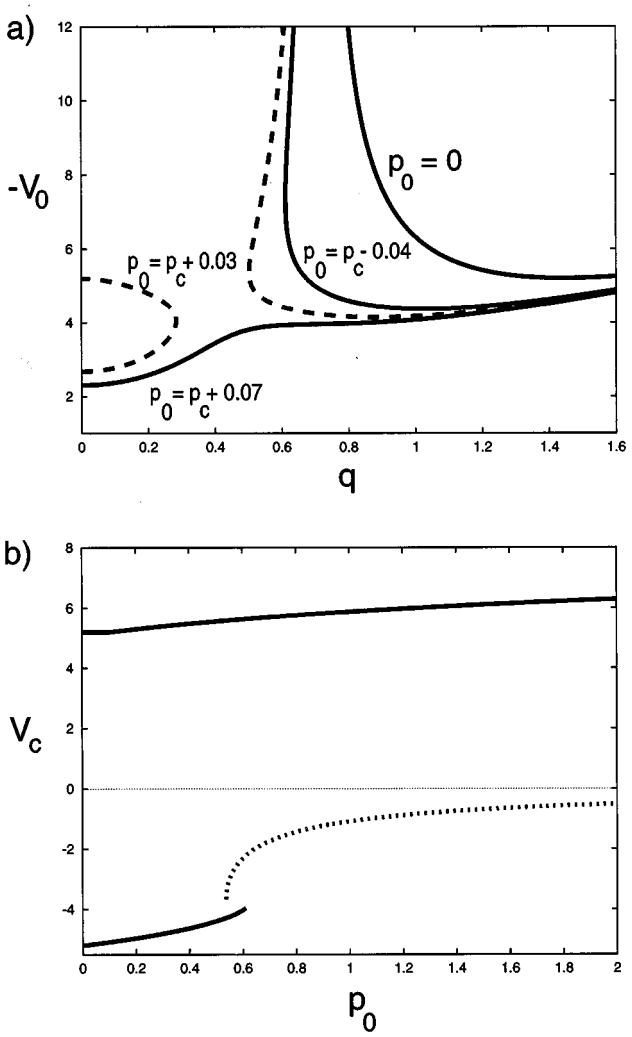

FIG. 3. The neutral curve (a) and the comparison of convective and Frederiks instabilities (b) just like in Fig. 2 but for negative dielectric anisotropy $\epsilon_a = -0.38\epsilon_0$, where $p_c = 0.54$.

B. dc electroconvection

The existence of a finite polarization also has a profound influence on the dc electroconvective instability. Without a polarization p_0 (smectic-*C* phase) the sign of the dc voltage is arbitrary and the threshold for the dc EC depends on V_0^2 only. This behavior is changed by the presence of the polarization **P** in smectic-C^*. Now **E** parallel to **P** ($V_0 > 0$) is energetically preferred to the case **E** antiparallel to **P** ($V_0 < 0$) (cf. Fig. 1) indicating that the basic state is more stable in the former situation than in the latter one. Thus, one can expect the dc EC threshold to increase (decrease) with p_0 for $V_0 > 0$ (< 0), which indeed has also been found numerically for rigid boundaries [cf. the solid curves in Figs. 2(b) and 3(b)].

This can also be understood analytically. Assuming stationary instabilities (a Hopf bifurcation has not been found in our numerical studies), we get a quadratic equation for $V_0(q)$, i.e., $b_1 V_0^2 + b_2 p_0 V_0 + b_3 = 0$, which is written down explicitly in Appendix B for the special case $\epsilon_a = 0$ and the stress-free boundary conditions. The interesting point is that it contains a linear term proportional to p_0. Thus, in contrast to the smectic-*C* case, in the smectic-C^* phase the neutral curve for dc EC is no longer symmetric with respect to $V_0 \to -V_0$.

This simple threshold condition also explains, why for finite p_0 values the range of existence of the dc EC is larger than for zero p_0. Real values for V_c are only possible, if $p_0^2 b_2^2 > -4 b_1 b_3$. Thus for zero p_0 the product $b_1 b_3$ must be negative, while for large enough p_0 also positive values of $b_1 b_3$ lead to an instability threshold. In particular, for a large enough and destabilizing polarization (**E** antiparallel to **P**, $V_0 < 0$), an electroconvective instability is possible, even if $\epsilon_a \leqslant 0$ and $\sigma_a < 0$. In this situation the planar basic state is stable within the simple Carr-Helfrich mechanism ($p_0 = 0$), but the destabilization due to p_0 overcomes the stabilization due to negative dielectric and conductive anisotropies.

C. dc electroconvection vs Frederiks transition

To predict the behavior of a smectic film under external electric fields, one has to take into account both, a Frederiks type ($q_c = 0$) and an EC instability ($q_c > 0$).

For $p_0=0$ and large positive values of ϵ_a the splay Frederiks transition always has a lower threshold than electroconvection (see, e.g., Ref. [23]). However, the threshold for the splay Frederiks transition diverges in the limit $\epsilon_a \to 0$, but below an intermediate (i.e., crossover) value of ϵ_a EC has a lower threshold than the Frederiks transition.

For finite p_0 the competition between both instabilities is shown in Figs. 2 and 3 for positive and negative ϵ_a, respectively. In these and the following figures the EC curves have been calculated using realistic (rigid) boundary conditions, but there are no qualitative differences to the case of free boundary conditions.

For a positive ϵ_a and for $V_0>0$ there are two minima in the neutral curve [Fig. 2(a)], where the EC threshold (at finite q_c) is lower for large values of p_0. In the case of $V_0<0$ and large p_0 the minimum of the neutral curve at finite q_c ceases to exist and the (general) Frederiks transition is the only possible instability. At small values of p_0 there is a crossover between the Frederiks instability and EC, where the two minima in the neutral curve correspond to the same value of V_0. At this codimension-two point the two instabilities with $q_c=0$ and $q_c>0$ coexist and nonlinearities, neglected in the calculation of the threshold, will decide, which structure actually survives. This is found numerically to take place at $p_r=0.25$ and $V_c>0$ for $\epsilon_a=0.6\epsilon_0$, while for a smaller (but still positive) dielectric anisotropy this point is shifted into the domain with $V_c<0$.

A slightly different scenario is found in the range $\epsilon_a<0$. If $V_0>0$ or if $V_0<0$ and $p_0<p_c$ [defined in Eq. (5.3)], there is only EC and no Frederiks transition possible [cf. the curves $p_0=0$ and $p_0=p_c-0.04$ in Fig. 3(a)]. For $p>p_c$ (and $V_0<0$) a Frederiks transition (minimum at $q=0$) is possible, while EC (minimum at finite q) seizes to exist for p_0 slightly above p_c ($p_0=p_c+0.07$ in Fig. 3). However, immediately at the point, where the Frederiks transitions starts to exist, it has a lower threshold than EC [cf. in Fig. 3(a) the dashed, disconnected curve with two different minima]. Thus the two threshold curves do not cross (no codimension-two point) and at p_c the (absolute value of the) threshold voltage jumps down from the EC value to the Frederiks value. Of course, for a different choice of material parameters (e.g., σ_a or ϵ_a) the Frederiks threshold could be higher than the EC threshold at p_c leading at some $p_r>p_c$ to a crossover (codimension-two point) between EC and Frederiks transition quite similar to the case of positive ϵ_a.

VI. ac INSTABILITIES

A. Harmonic regimes

For $p_0=0$ (smectic-C phase) the harmonic solutions of Eq. (4.37), $l=even$, ($\mathbf{U}_{\mathrm{harm,anti}}$,$\mathbf{U}_{\mathrm{harm,sym}}$) are each decomposed into two independent classes (called A and B in [12]) representing the conductive and dielectric regimes, respectively. This is due to the additional symmetry described by Eq. (4.27), which implies that on one branch (A) the excited modes are only the odd harmonic ones $l=2,6,10,\ldots$ of the electric variable ϕ and the even harmonic ones $l=0,4,8,\ldots$ of the hydrodynamic variables θ and v_z, and vice versa for branch B. In the first case, the lowest mode at the onset of instability consists of a harmonically oscillating electric charge density while the hydrodynamic variables are effectively constant. Therefore the regime is called conductive in agreement with the Carr-Helfrich explanation for the nematic case. In the second, dielectric case, the excitation is just the opposite with harmonically oscillating lowest modes for the hydrodynamic variables θ and v_z and a constant electric variable ϕ (in the lowest mode).

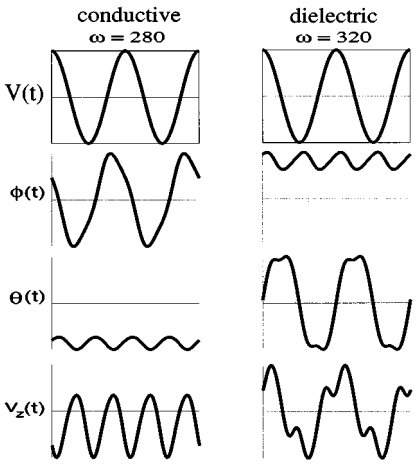

FIG. 4. The time dependence of the field variables is shown at the onset of electroconvection in the Sm-C phase (without macroscopic polarization). The temporal variations of the fields at the cell center ($z=0$) are plotted in arbitrary units for the conductive ($\omega=280$) and dielectric regime ($\omega=320$).

For small values of the parameter $\sigma_\perp d^2$ the higher order (temporal) modes are considerably excited at the onset of instability, as can be seen from Fig. 4. Increasing $\sigma_\perp d^2$ there remain large contributions from these higher harmonics only near the transition from the conductive to the dielectric regime [5,27].

In Fig. 5 the neutral curves for the class ($\mathbf{U}_{\mathrm{harm,sym}}$), are

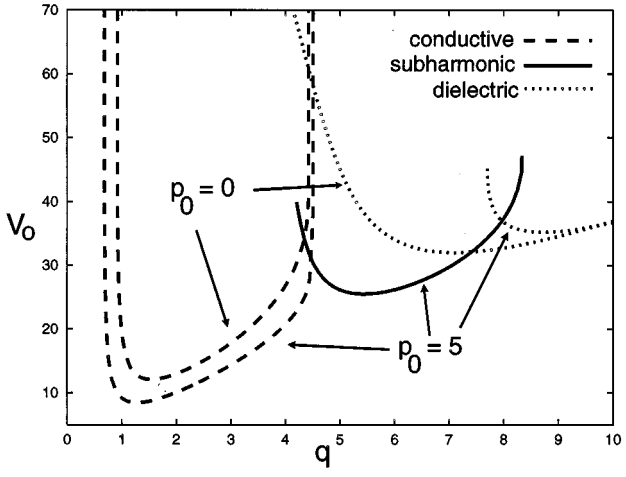

FIG. 5. Neutral curves $V_0(q)$ are given for two different values of the polarization ($p_0=0$ and 5) at the frequency $\omega=180$ of the applied voltage. The upper (lower) curve in the conduction regime (dashed lines) and the lower (higher) one in the dielectric regime (dotted lines) are calculated for $p_0=0$ ($p_0=5$). For finite polarizations the additional subharmonic regime occurs at intermediate q values (solid line).

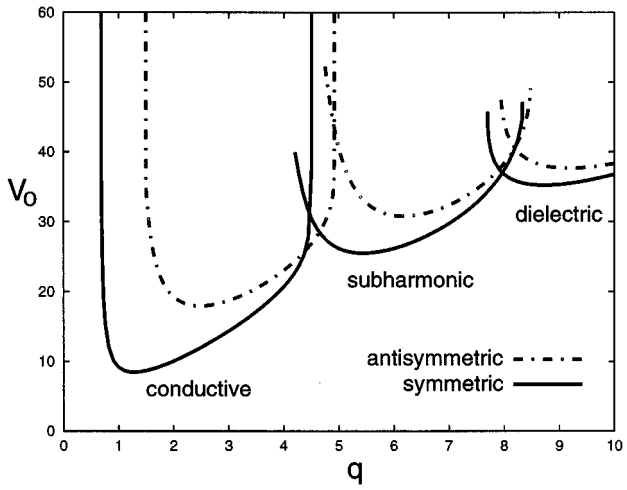

FIG. 6. Three different instability regimes: (a) The conductive, (b) the subharmonic and (c) the dielectric regime. The solid lines show the neutral curves $V_0(q)$ for branches symmetric under z reflection Eq. (4.23) while the dash-dotted lines belong to antisymmetric solutions. Here the parameters (applied ac frequency $\omega=180$ and spontaneous polarization $p_0=5$) are chosen such that the lowest minimum of the neutral curves belongs to the conductive regime.

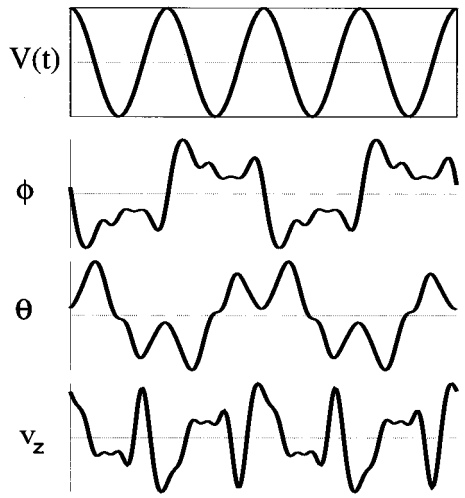

FIG. 7. The time dependence of the field variables is shown at the onset of EC in the Sm-C^* phase (with macroscopic polarization). The fields at the cell center ($z=0$) are plotted in arbitrary units for the frequency $\omega=390$ of the applied voltage. The dynamics of the system is $2T$ periodic only, although the driving force $V(t)$ is T periodic.

plotted for two different values of the polarization, $p_0=0$ and 5 at the frequency $\omega=180$ of the applied voltage. For vanishing polarization the neutral curve has two branches with one minimum each, where the dashed curve belongs to the conductive regime and the dotted curve to the dielectric regime.

For finite values of the spontaneous polarization, p_0, the symmetry of Eq. (4.27) no longer exists and all harmonic modes are coupled. This means, for instance, that the even harmonic modes ($l=2,6,10,\ldots$) of the induced potential ϕ are also exited in the conduction regime. The amplitudes of those additionally excited modes increase with increasing values of p_0. The same holds for the odd harmonic modes in the dielectric regime. Similar changes occur for the two other hydrodynamic variables θ and v_z.

Despite the polarization induced excitations of even and odd modes we still call the two regimes conductive and dielectric, respectively, due to their origin. With increasing values of p_0 the minimum of the neutral curve in the conduction regime (dashed) is shifted to lower, and the dielectric one (dotted) to higher, critical voltages and critical wave numbers q_c. For higher values of p_0 a new minimum of the class ($\mathbf{U}_{\text{subh,sym}}$) occurs (Fig. 5), which will be discussed in Sec. VI B.

For nematic liquid crystals it has been shown that the branches belonging to ($\mathbf{U}_{\text{harm,anti}}$) have always a higher threshold than those for ($\mathbf{U}_{\text{harm,sym}}$) (see Refs. [8,12,27] and references therein). This is still true for finite polarizations in the C^* phase (Fig. 6). In addition also the antisymmetric subharmonic branch ($\mathbf{U}_{\text{subh,anti}}$) shows a higher threshold voltage than the symmetric subharmonic one ($\mathbf{U}_{\text{subh,sym}}$). Thus all the antisymmetric (dash-dotted) solutions are not involved in the onset of convection and will not be considered any further.

B. Subharmonic ac regime

The subharmonic regime corresponds to the class ($\mathbf{U}_{\text{subh,sym}}$) of solutions, where at the onset of convection all variables ϕ, θ, and v_z are oscillating with half the frequency ($l=1$) and appropriate higher harmonics ($l=3,5,7,\ldots$) of the applied voltage. In this regime the temporal behavior of the fields ϕ,θ,v_z is shown in Fig. 7 at threshold and at the cell center ($z=0$). For the chosen parameter set higher harmonics are considerably excited.

For $p_0=0$ the subharmonic regime is strictly prohibited by the symmetry (4.27). The absence of this symmetry for finite polarizations in turn allows for subharmonic solutions (Figs. 5,6), which break spontaneously the discrete time translational symmetry of the driving voltage (T periodicity), since they are only $2T$ periodic (subharmonic).

Changing the frequency ω the three minima of the neutral curve (Fig. 5) are shifted relative to each other, such that any of them can be the absolute minimum, i.e., the threshold V_c for a certain frequency range. The critical threshold voltages, $V_c(\omega)$ and the associated critical wave vectors $q_c(\omega)$ are plotted for each regime as a function of frequency ω in Fig. 8 for two different values of the polarization p_0.

For sufficiently high values of p_0 the neutral curve belonging to the subharmonic regime ($\mathbf{U}_{\text{subh,sym}}$) has the lowest minimum for a certain frequency range (solid line in Fig. 8). It always appears at intermediate frequencies, between the conductive and dielectric regime. Fig. 8(b) shows the critical wave number q_c as a smooth function of the external frequency within a given regime, but with discontinuous jumps when the marginal stability switches from one regime to another. Again only two regimes are present for $p_0=0$, but three for large enough p_0.

Although there is no simple mechanism that could explain, why a subharmonic regime exists as the marginally stable solution, the following remarks may help the intuition. With $p_0=0$ the sign of V_0 is undefined and it is rather V_0^2

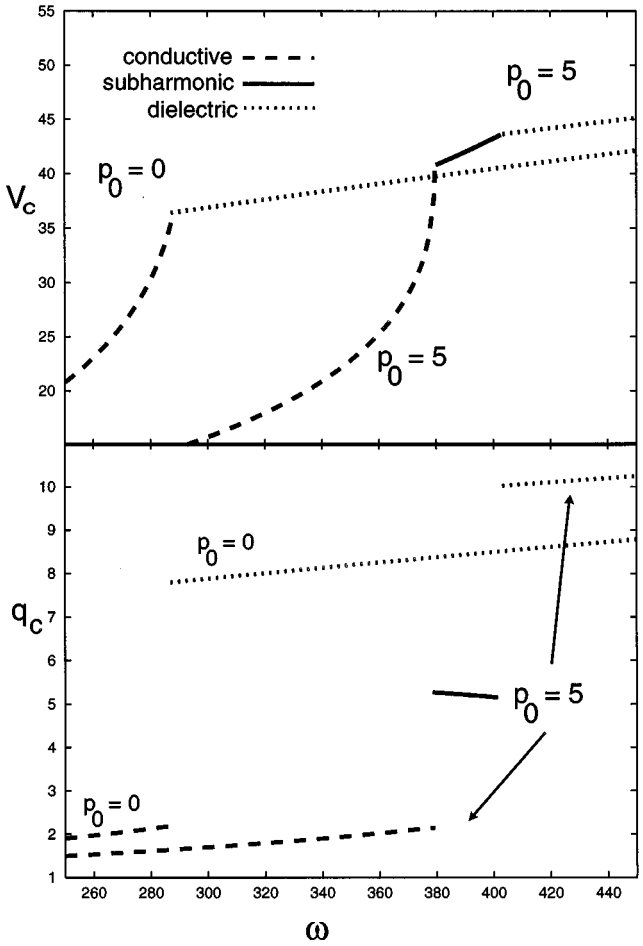

FIG. 8. Onset of instability: (a) The critical voltages $V_c = V(q_c)$, (b) the critical wavelengths q_c, of the three regimes as a function of the applied ac frequency. For low or vanishing polarization p_0 there are only two regimes, while for $p_0 > 4.5$ (for the parameters chosen) there is in addition the subharmonic regime at intermediate frequencies. At those frequencies, where the instability switches from one regime to the other, the critical wave vector shows a jump.

that governs the instability thresholds. A finite p_0, however, introduces contributions linear in V_0 as has been shown explicitly in the dc case (Sec. V). Thus for sinusoidal voltages $V(t)$ the fields may oscillate either with half the frequency of $V(t)^2$ or $V(t)$, depending on the influence of the different destabilizing forces. For very large threshold voltages, such as in the dielectric regime, contributions in the director relaxation time being quadratic in the voltage V^2 win over those effects linear in V. At small frequencies in the conduction regime the threshold is relatively small and the impurity charges can follow the action of the external field immediately while leaving the director orientations roughly unchanged. In both cases the fields oscillate in a subharmonic fashion with respect to V^2.

The frequency range of the conduction regime is always bounded from above by the inverse charge relaxation time. Beyond that frequency the charges get out of phase and if immediately beyond that frequency the contributions $p_0 V$ to the director relaxation time are more important than those proportional to V^2 then the subharmonic regime may have a

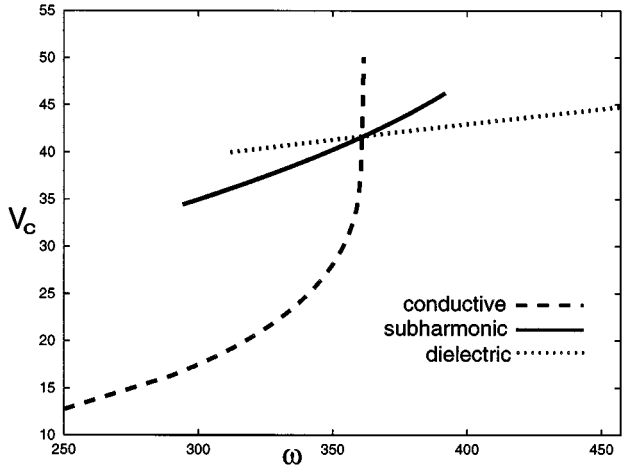

FIG. 9. Codimension-three point: At the minimal value of the polarization ($p_0 = 4.5$ for the parameters chosen), for which the subharmonic regime exists, the three different regimes have equal critical voltages at a certain external ac frequency $\omega_3 \approx 361$. This is a codimension-three point.

lower threshold than the dielectric one. With further increasing frequency also the threshold increases and therefore at large frequencies V^2 dominates the V effects and the dielectric regime is favored. Using these qualitative arguments the subharmonic regime can only occur as an additional regime between the conduction and the dielectric regime.

C. Codimension-three bifurcation

The value of p_0 can be seen as a third control parameter of the system in addition to the amplitude, V_0, and frequency, ω, of the applied voltage. For large polarizations the subharmonic threshold curve $V_c(\omega)$ intersects both, the conductive and the dielectric threshold curves, at two codimension-two points (indicated in Fig. 8). If p_0 is lowered, these two codimension-two points approach each other and finally merge (cf. Fig. 9). We have found numerically that this coalescence happens just at the point, where also the conductive and dielectric thresholds intersect. This codimension-three point is shown in Fig. 9 with the parameter values $p_3 = 4.5$, $\omega_3 = 361$, $V_3 = 41.5$ and for the material parameters given in Appendix A. Here all three regimes coexist and a competition of three solutions having different wavelengths should be seen in experiments. For $p_0 < p_3$ the subharmonic regime disappears. (The actual value of p_3 depends obviously on the material parameters.) This scenario seems to be generic, since near this codimension-three point the threshold curves $V_c(\omega)$ are nearly straight lines, where the conductive and dielectric curve have the largest and smallest slope, respectively.

Increasing however the polarization p_0 well beyond p_3 the cutoff frequency of the conductive regime is shifted to higher values and the threshold and critical wavelength at a fixed frequency is lowered further. The subharmonic regime appears always after the cutoff of the conductive regime for high values of p_0 and is extended to much higher frequencies at the cost of the dielectric regime. E.g., for $p_0 = 50$ the cutoff frequency is at $\omega \approx 13000$ while for the conductive regime we find typically rather small threshold values

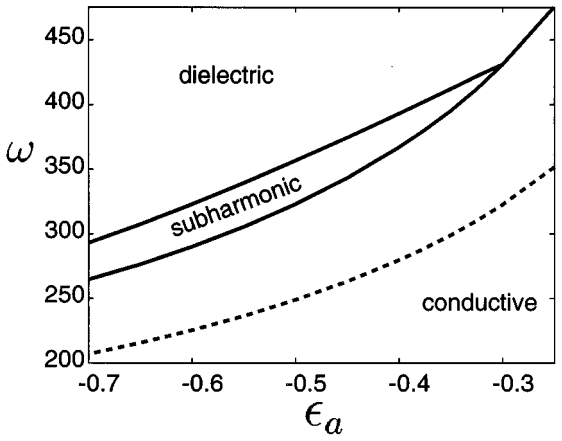

FIG. 10. The existence range of the subharmonic regime at various ac frequencies ω as a function of the dielectric anisotropy for $p_0=5$ and $\sigma_\perp=133$ fixed [both in dimensionless units cf. Eqs. (4.10) and (4.11)] and $\epsilon_\perp=5.25$. The dashed line describes the codimension-two line between the conductive and the dielectric regimes for $p_0=0$.

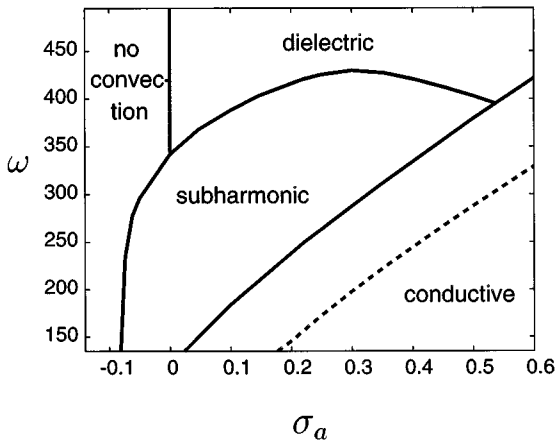

FIG. 11. The solid lines indicate the existence ranges of the different instability regimes at various ac frequencies as a function of the conduction anisotropy σ_a for $p_0=5$ and $\sigma_\perp=133$ and $\epsilon_\perp=5.25$; $\epsilon_a=-0.38$. The dashed line describes the codimension-two line between the conductive and the dielectric regimes for $p_0=0$.

$q_c\approx 0.15$ and $V_c\approx 0.5$ at $\omega=200$. The observation of such very small wave numbers should not be confused with the Frederiks transition ($q\equiv 0$, which does not occur for $\epsilon_a<0$).

D. Parameter dependencies

The frequency range, where the subharmonic regime has the lowest threshold, depends not only on the polarization but also on the values of the other material parameters and on the film width. To design an experiment for investigating the subharmonic regime it is helpful to know, for which geometric and material parameters the subharmonic regime can be observed most likely. All results described in the previous sections of this work have been calculated for the values given in Appendix A. The electroconvective instability is especially sensitive to changes in the electrical anisotropies ε_a and σ_a [12,23,27,28]. Therefore we consider the influence of variations of these quantities on the existence range of the subharmonic regime.

(i) A scaling of the two dielectric constants $\epsilon_{\perp,\parallel}$ by the same factor will only shift the threshold voltage due to Eq. (4.5). Large positive values of ϵ_a will not lead to EC ($q_c\neq 0$), since the threshold for the Frederiks transition becomes the lower one. For $\epsilon_a<0$ changes of $\epsilon_\parallel/\epsilon_\perp$ (or $\epsilon_a/\epsilon_\perp$) have rather subtle implications, which cannot be understood from the scaling of the Eqs. (4.12–4.14) alone, but numerical calculations have to be used. Thus we have computed thresholds curves $V_c(\omega)$ with $p_0=5$ for different values of ϵ_a (cf. Fig. 10). The different regimes are separated by codimension-two lines, which intersect at the codimension-three point. The range of the subharmonic regime widens with ϵ_a becoming more negative, while above $\epsilon_a=-0.3$ (for the parameters used) the subharmonic regime ceases to exist.

(ii) We investigated the dependence on σ_a by keeping $\sigma_\perp$ constant and changing the value of $\sigma_\parallel$. Increasing values of σ_a enforce the ability of space charges to follow the applied alternating field up to higher frequencies according to the Carr-Helfrich mechanism [11,13]. Thus the cutoff frequency of the conductive regime increases approximately proportional to σ_a while the dielectric regime is only slightly affected. This is shown for $p_0=0$ by the dashed line in Fig. 11. Similar behavior is found for a finite polarization (solid lines) although for $\sigma_a/\sigma_\perp<0.55$ (for the parameters chosen) the subharmonic regime squeezes in between the two other regimes. The threshold voltages of the conductive and the dielectric regimes diverge by approaching $\sigma_a\to 0$ according to the Carr-Helfrich mechanism causing smaller values of the anisotropy σ_a to favor the subharmonic regime. Furthermore the subharmonic regime exists even for (slightly) negative values of the anisotropy σ_a. The same has been found for an applied dc voltage (cf. Sec. V C). Increasing p_0 will again lead to a larger frequency range of the subharmonic instability and the subharmonic regime will exist to even larger values of σ_a than indicated in Fig. 11.

(iii) In Sec. IV A the scaling was chosen such that variations of the film width d do not change the (dimensionless) viscosities and elastic constants, which are rather difficult to vary experimentally. This means that mainly the same compounds can be used for different film widths d. On the other hand the frequency of the applied AC voltage as well as the spontaneous polarization p_0 (by adding chiral molecules) or the electric conductivity σ (by adding dopants) can easily be adjusted in an experiment. I.e., the influence of the film width d, showing up in the (dimensionless) quantities $\sigma\sim d^2$, $p_0\sim d$, and $\omega\sim d^2$ [cf. Eqs. (4.4), (4.10), and (4.11)] can be balanced by appropriate changes of the physical quantities. Varying both, the film width and the material parameters, the threshold voltage, the critical wavelength and the frequency can be brought into a range accessible to experiments.

VII. CONCLUSION

In this paper we have analyzed the linearized electrohydrodynamics of a freely suspended smectic-C^* liquid crystal film. We have neglected the biaxiality of this phase and have described it as being isomorphic to a two-dimensional nem-

atic with an additional spontaneous polarization. The qualitatively different effects due to the spontaneous electric polarization are the main topic of this work. We predict electroconvection for thin smectic films as already known from bulk nematics, but with some completely new and experimentally accessible features. For applied dc voltages a spontaneous polarization leads to a stabilization or a destabilization of the planar ground state (i.e., to an increase or decrease of the threshold for electroconvective instabilities) depending on whether the polarization is parallel or antiparallel to the driving field. A generalized Frederiks transition including torques due to the polarization is possible even for negative or vanishing dielectric anisotropy and its influence on the observation of pattern forming instabilities has been discussed.

For applied ac voltages the well-known conductive and dielectric regimes, which are governed by a harmonic movement of all variables at the onset of convection, are mainly shifted to lower and higher thresholds, respectively, due to the finite polarization. A different class of solutions, however, moving subharmonically at the onset, becomes possible due to the polarization. Detailed investigations of the dependence on the parameters of this different regime give the trends for which materials the subharmonic regime will occur most likely. The frequency range of the subharmonic regime depends mainly on the polarization, dielectric and the conduction anisotropy as well as the width d of the film. The major trends are: Moderate values of the polarization, small width d, small anisotropies of the conductivity, negative values of the dielectric anisotropy and small values of σd^2 are favorable for the subharmonic regime. It is predicted that electroconvection can also occur for negative anisotropy of the conductivity due to the polarization. The possibility of an oscillatory Hopf bifurcation was considered in all numerical calculations but was never found for any parameter regime as discussed in Sec.VI D.

The nonlinear treatment of the various stationary bifurcations (especially near the codimension-three point) will be the subject of future work, which will also include a fully three-dimensional calculation taking into account film undulations and the helical structure of the polarization. Finally we have made explicit suggestions for experiments to find the subharmonic regime.

ACKNOWLEDGMENTS

We would like to thank the Deutsche Forschungsgemeinschaft for partial support of this work through the Schwerpunkt ''Strukturbildung in dissipativen kontinuierlichen Systemen: Experiment und Theorie im quantitativen Vergleich.''

APPENDIX A: MATERIAL PARAMETERS

All numerical calculations were done with material parameters listed in Table I, if not mentioned otherwise in the text. See Secs. VI C and VI D for further details. Note that in this Appendix all quantities are given in real units and correspond to the unprimed quantities, e.g., σ and p_0.

TABLE I.

Parameter	Symbol	Value	Unit
Elastic constants	K_1	6.66	10^{-12} N
	K_2	4.2	
	K_3	8.61	
Viscosities	α_1	-18.1	$10^{-3}\frac{\text{kg}}{\text{m s}}$
	α_2	-110.4	
	α_3	-1.1	
	α_4	82.6	
	α_5	77.9	
Dielectric constants	ϵ_0	8.85	$10^{-12}\frac{\text{A s}}{\text{V m}}$
	ϵ_a/ϵ_0	-0.38	
	$\epsilon_\parallel/\epsilon_0$	4.87	
	$\epsilon_\perp/\epsilon_0$	5.25	
Conductivities	$\sigma_\parallel$	5.6	$10^{-8}\frac{1}{\Omega\ \text{m}}$
	$\sigma_\perp$	3.7	
	σ_a	1.9	
Polarization	p_0	0 . . . 1	$10^{-9}\frac{\text{C}}{\text{m}^2}$

APPENDIX B: dc ELECTROCONVECTION FOR $\epsilon_a = 0$

To analyze analytically the influence of p_0 on EC, we present here the neutral curve $V_0(q)$ for dc EC for free boundaries and $\epsilon_a=0$. The ansatz (4.28) for $\hat{\mathbf{u}}$ of the general solution Eq. (4.25) is reduced to three time-independent functions $\mathbf{u_0}=(\phi_0,\theta_0,v_{z0})$, i.e., $l=0$ in (4.28). For free boundaries it is sufficient to take along only the lowest order $(m=1)$ in the space expansion (4.29)–(4.31). The generalized eigenvalue problem (4.36) for $\mathrm{Re}(\sigma)=0$ is then reduced to $0=\mathsf{L}_1\cdot\mathbf{X}$, where L_1 is a 3×3 matrix. Nontrivial solutions are obtained for $\det\mathsf{L}_1=0$. From Eqs. (4.12)–(4.14) we obtain

$$V=\frac{p_0 b_2}{2b_1}\left[-1\pm\left(1+\frac{4b_1b_3}{p_0^2b_2^2}\right)^{1/2}\right], \tag{B1}$$

with

$$b_1=\frac{\sigma_a}{\sigma_\perp}q^2\frac{(\alpha_3-\alpha_2q^2)(1+q^2)}{(\eta_c q^4+2\hat{\eta}q^2+\eta_b)(q^2\sigma_\parallel/\sigma_\perp+1)}, \tag{B2}$$

$$b_2=\frac{\sigma_a q^2}{\sigma_\parallel q^2+\sigma_\perp}-1-\frac{\alpha_2q^2-\alpha_3}{\eta_c q^4+2\hat{\eta}q^2+\eta_b}q^2, \tag{B3}$$

$$b_3=1+q^2K_3/K_1. \tag{B4}$$

One can easily see that the threshold exists as long as the expression under the square root stays positive, which is the case for $p_0^2b_2^2>-4b_1(1+q^2K_3/K_1)$. For $p_0=0$, b_1 has to be negative, which implies σ_a to be positive. If $p_0>0$, even negative values of σ_a are possible, where the critical value

for the conductivity anisotropy up to which dc EC exists, scales like $\sigma_a \propto -p_0^2$. In the general case of finite ϵ_a the formulas become more involved, but there is still a condition on the material parameters (mainly on p_0, σ_a and ϵ_a) for the existence of the dc EC. This means, on the other hand, that there are parameter ranges (positive and/or negative σ_a and/or ϵ_a), where EC exists for large enough p_0, but not for $p_0 = 0$.

[1] *Propagation in Systems Far from Equilibrium*, edited by J. E. Wesfred, H. R. Brand, P. Manneville, and G. Albinet (Springer, New York, 1988).

[2] *Spatio-Temporal Patterns in Nonequilibrium Complex Systems*, Vol. XXI of *Santa Fe Institute Studies in the Sciences of Complexity*, edited by P. Cladis and P. Palffy-Muhoray (Addison-Wesley, New York, 1995).

[3] M. C. Cross and P. C. Hohenberg, Rev. Mod. Phys. **65**, 851 (1993).

[4] P. Oswald, J. Bechhoefer, and F. Melo, Mat. Res. Bulletin **16**, 38 (1991).

[5] W. Zimmermann, Mat. Res. Bulletin **16**, 46 (1991).

[6] L. Kramer and W. Pesch, Annu. Rev. Fluid Mech. **27**, 515 (1995).

[7] I. Rehberg *et al.*, in *Festkörperprobleme 29*, edited by Fritz Sauter (Vieweg, Braunschweig, 1989), p. 35.

[8] S. Kai and W. Zimmermann, Prog. Theor. Phys. Suppl. **99**, 458 (1989).

[9] H. R. Brand, P. E. Cladis, and P. L. Finn, Phys. Rev. A **31**, 361 (1985).

[10] S. W. Morris, J. R. de Bruyn, and A. May, Phys. Rev. A **44**, 8146 (1991).

[11] P. G. de Gennes and J. Prost, *The Physics of Liquid Crystals* (Clarendon, Oxford, 1993).

[12] W. Zimmermann, in *Defects, Singularities and Patterns in Nematic Liquid Crystals, NATO Advanced Study Institute Series*, edited by J. M. Coron, F. Helen, and J. Ghidaglia (Kluwer, Dordrecht, Netherlands, 1991).

[13] W. Helfrich, J. Chem. Phys. **51**, 4092 (1969).

[14] C. Rosenblatt, R. Pindak, N. Clark, and R. B. Meyer, Phys. Rev. Lett. **42**, 1220 (1879).

[15] S. Faetti, L. Fronzoni, and P. Rolla, J. Chem. Phys. **79**, 1427 (1983).

[16] W. Zimmermann, S. Ried, H. Pleiner, and H. R. Brand, Europhys. Lett. **33**(7), 521 (1996).

[17] S. W. Morris, J. R. de Bruyn, and A. May, J. Stat. Phys. **64**, 1025 (1991).

[18] H. Pleiner and H. R. Brand, in *Pattern Formation in Liquid Crystals*, edited by A. Buka and L. Kramer (Springer, Berlin, 1995).

[19] W. Zimmermann, H. Pleiner, and H. Brand (unpublished).

[20] D. Forster, T. C. Lubensky, P. C. Martin, J. Swift, and P. S. Pershan, Phys. Rev. Lett. **26**, 1016 (1971).

[21] P. C. Martin, O. Parodi, and P. S. Pershan, Phys. Rev. A **6**, 36 (1972).

[22] H. R. Brand and H. Pleiner, Phys. Rev. A **35**, 3122 (1987).

[23] E. Bodenschatz, W. Zimmermann, and L. Kramer, J. Phys. (Paris) **49**, 1875 (1988).

[24] G. Iooss and D. D. Joseph, *Elementary Stability and Bifurcation Theory* (Springer, Berlin, 1980).

[25] S. Chandrasekhar, *Hydrodynamic and Hydromagnetic Stability* (Oxford University Press, London, 1961).

[26] V. Frederiks and V. Zvetkoff, Sov. Phys. **6**, 490 (1934).

[27] L. Kramer, E. Bodenschatz, W. Pesch, W. Thom, and W. Zimmermann, Liq. Crys. **5**, 699 (1989).

[28] W. Zimmermann and L. Kramer, Phys. Rev. Lett. **55**, 402 (1985).